# Acoustic holograms for homogeneous hyperthermia over several tumor spheroids

Diana Andrés *, Ian Rivens †, Petros Mouratidis †, Noé Jiménez *, Francisco Camarena *
, Gail ter Haar †
*Instituto de Instrumentación para Imagen Molecular, Universitat Politècnica de València, Spain
Email: diaanbau@upv.es
†Institute for Cancer Research (ICR), London, SM2 5NG, UK

2023 IEEE International Ultrasonics Symposium (IUS) | 979-8-3503-4645-9/23/$31.00 ©2023 IEEE | DOI: 10.1109/IUS51837.2023.10307873

***Abstract*—In this work we use 3D printed holographic lenses to enlarge the natural focus of a curved transducer with the aim of producing a uniform region of iso-thermal dose. With this system, we exposed several U87-MG glioma cell spheroids, located inside an IEC tissue mimicking phantom, to a uniform and real-time monitored temperature. Spheroids were exposed with this system until different thermal iso-effective doses (7.5, 30, 60, 120 CEM43) (TIDs) were reached. Also, the effects of ultrasound-delivered hyperthermia on the response of these spheroids were compared with heating using a polymerase chain reaction (PCR) thermal cycler in terms of viability and growth measured on a 10-day schedule. Using acoustic holograms designed to deliver iso-thermal doses, we observe a 6 mm wide uniform region of hyperthermia over the three targets, with temperature differences of less than 3%. In addition, tumor spheroid responses show that ultrasound delivered hyperthermia is more damaging than PCR heating for TIDs $\geq$ 30 CEM43. This system could help in future in-vitro studies of hyperthermia delivered with ultrasound.**

***Index Terms*—acoustic holograms; acoustic lenses; ultrasound hyperthermia; tumour spheroids; thermal dose.**

## I. Introduction

Ultrasound hyperthermia is used as a chemo- or radio- sensitizer in cancer treatment. It differs from other hyperthermia delivery methods in its ability to increase temperature locally inside the body in a non-invasive way [1]. The energy of the acoustic wave is concentrated at the focus of the system and it produces local tissue heating mainly due to the activation of thermoviscous processes [2].

Ultrasound-induced hyperthermia can be delivered using a focused transducer, which concentrates the acoustic energy into a focal spot. To cover targets larger than the transducer focus and get a uniform region of hyperthermia, repeated sonications in adjacent positions are needed [3], [4]. Also, complex and expensive phased-array technology can be used to steer the focus rapidly [5], [6]. Recently, a novel technique based on 3D-printed acoustic lenses or holograms coupled to ultrasound transducers are used to shape and control the acoustic field. These lenses can compensate for the phase distortions produced by aberrating layers, such as the skull, producing aberration-corrected focal spots [7] or therapeutic acoustic images of arbitrary shape [8]. Holographically-designed lenses are under study for cell patterning [9], cavitation pattern generation [10], and local blood-brain barrier opening in the brain [11]. Acoustic holograms have also been recently used to generate arbitrary thermal patterns [12]. However, using this approach, the temperature rise is not uniform throughout the whole target.

To study how hyperthermia affects tumor cells, 3D cell aggregates (i.e. spheroids) are considered to better mimic the behaviour of in-vivo tumors than 2D monolayers [13]. These studies were carried out using a polymerase chain reaction (PCR) thermal cycler, showing important differences between 3D and 2D tumor models [14]–[16]. Nevertheless, heating using ultrasound is presumed to present non-thermal mechanisms that may also affect cell growth, such as cavitation [17] or acoustic radiation forces [18].

In this work we want to study how ultrasound-delivered hyperthermia affects tumor spheroids in-vitro and compare its response to those treated using PRC heating. We have designed a system based on acoustic holograms coupled to a ultrasound transducer with the aim to provide a region of uniform hyperthermia over complex targets. Two holographic lens were studied: the first one was designed to provide similar acoustic peak pressure over the target locations, whilst the second one was thought to create a region of uniform temperature rise over the target area. Both lenses were acoustically and thermally characterized both experimentally and with numerical modelling. To expose several tumor spheroids at the same time to a controlled thermal iso-effective dose (TID), a holder filled with an ultrasound absorbing (tissue mimicking) gel phantom was made. The holder presented three wells to contain the spheroids and three thermocouples beneath them to have real-time monitoring of the temperature and TID delivered. Several U87-MG cell spheroids were treated with this system to fixed TIDs and their response (growth and viability) was compared to those treated with a PCR thermal cycler [19].

## II. Materials and Methods

The system used in this work consisted on a focused ultrasound transducer (H148-MR Sonic Concepts, WA, USA) with 63.2-mm radius of curvature, 64-mm outer diameter, 23-mm inner hole diameter and 1.66 MHz central frequency, coupled to a 3D-printed holographic lens. Lenses were designed using time-reversal methods by setting virtual sources in the region of interest and tuning their amplitude and phase. Two approaches were explored to design the optimal lens for the purpose of treating several tumor spheroids to the same TID:

Authorized licensed use limited to: UNIVERSIDAD POLITECNICA DE VALENCIA. Downloaded on February 24,2025 at 15:23:24 UTC from IEEE Xplore. Restrictions apply.

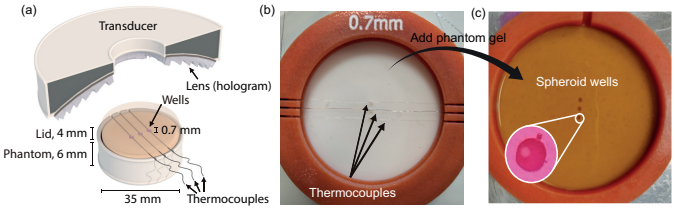



Fig. 1. Holographically designed lens, high intensity focused ultrasound transducer and absorbing gel spheroid holder. (a) Schematic of the spheroid exposure system with its dimensions. (b) The mould used to form the absorbing gel phantom with the three thermocouples. (c) The mould filled with IEC tissue mimicking gel, with 3 miniature wells into which a spheroid could be placed (inset). A gel lid closes the phantom

an iso-pressure strategy which aimed to an equal acoustic peak pressure at each spheroid location (using 3 virtual sources), and an iso-thermal strategy in which we pursued a uniform region of hyperthermia over the spheroids region considering heat diffusion and perfusion (using 7 virtual sources). Acoustic and thermal simulations were performed with the software k-Wave [20]. Lenses were designed following an adapted version of the procedure described in [8] using spherical coordinates to match the shape of the focused transducer (see Ref. [12][Suppl. Mat.]).

The spheroids holder was designed with three wells of 10 mm diameter and 7 mm wide, spaced 2 mm apart. Three 300-$\mu$m diameter T-type thermocouples (COCO-003, Omega, UK) were located below the wells for calibration of the system and real-time temperature and thermal dose monitoring (TID was calculated as described in [21]). The holder was filled with IEC tissue mimicking phantom with a 3% Phenol red for better visualization and retrieval of the spheroids. Separate 4- mm thick gel lids were made to ensure the spheroids were fixed and surrounded of absorbing medium while exposing them. The system is shown in Fig, 1.

For simulations, the medium was considered to have acoustic water properties (temperature = 38 °C, density $\rho_0$ = 1000 kg/m$^3$, sound speed $c_0$ = 1520 m/s and attenuation coefficient $\alpha_0$ = 0.0023 dB/(cm-MHz$^2$). Designed lenses were 3D printed using VeroClear resin, whose properties were measured in the laboratory ($\rho_L$ = 1181 kg/m$^3$ and $c_L$ = 2525 m/s, and with acoustic absorption set to $\alpha_L$ = 1.65 dB/(cm-MHz$^\gamma$), using $\gamma$ = 1.1), and inserted with their corresponding geometry in the simulations. Thermal simulations were based on a pseudo-spectral time-domain solution of the Penne's bio-heat equation [22]. To characterize the spheroids holder, it was considered to be surrounded by water and its dimensions, thermal and acoustic properties were considered, matching those reported by the IEC standard (IEC 60601-2-37:2007) ($\rho_p$ = 1050 kg/m$^3$, $c_p$ = 1540 m/s, specific heat capacity $C_p$ = 3550 J/(kg · K), thermal conductivity $k_p$ = 0.52 W/(m · K). Heating times up to 10 minutes were simulated, with time steps of 0.5 s. All media initial temperature was set to 38 °C and at each time step the water temperature surrounding the phantom was set to this initial value to match experimental conditions.

Acoustic field validation was performed in a degassed-water tank using an hydrophone (HNA-0400, ONDA Corp (CA, USA)) mounted on a 3D positioning system (UMS, Precision Acoustics, Dorset, UK). The transducer was driven with sinusoidal pulsed-burst signals (40 cycles, PRF = 200 Hz, 40 mVpp) using a signal generator (33250A Agilent, Santa Clara, USA), after being amplified (A300, 55 dB, E&I, NY, USA). 20-times averaged signals were recorded with a digital oscilloscope (LeCroy 64Xi), using a time window of 20 $\mu$s after reaching steady state. Thermal experiments (for validation and tumor exposure) were done inside a 38- °C degassed-water tank, using a recirculation circuit consisting of a degasser (2.5 X 8 Liqui-Cel Membrane Contactor, 3M, NC, USA) connected to a vacuum line (27 in. Hg), a water chiller (HC-100A, Hailea, Guang-dong, China) and a water heater (GD 100, Grant scientific, Cambridgeshire, UK) placed in the exposure tank. Thermocouples were connected to module (NI-9213, National Instruments, Tx, USA) used in high resolution (1 measurement per second).

## III. RESULTS

For the iso-pressure lens we obtained peak positive pressures of 1.34 ±± 0.08, 1.12 ± 0.08 and 1.28 ± 0.03 MPa at each focus, with the transducer driven at 85 mVpp. Foci were deviated 0.1, -0.1 and -0.2 mm relative to their simulated locations on the y-axis and presented FWHM values of 0.85 ± 0.05, 0.89 ± 0.05 and 0.91 ± 0.05 mm. Maximum difference in acoustic pressure among foci is 15% (Fig. 2-(a)).

Thermal profiles recorded at each localised thermocouple are shown in Fig 2-(c). The maximum steady-state temperatures registered by each thermocouple were 48.0 ± 0.1, 48.7 ± 0.1 and 47.2 ± 0.1 °C, from left to right, respectively. Mean TID in was calculated as the mean value in measurements made between -0.5 and 0.5 mm around the central location for each thermocouple, and the error corresponds to its standard deviation. At each well, mean TIDs were 73 ± 13, 103 ± 14 and 38 ± 6 CEM$_{43}$, from left to right. Comparing this value in the central well with the others, gives a relative error of 29.1% for the one located at its left, and 63.1% at its right, while the difference between the left and the right wells was 47.9%.

For the iso-thermal lens we obtained peak positive pressures of 1.04 ± 0.09, 0.80 ± 0.08, 0.78 ± 0.08, 0.66 ± 0.08, 0.86 ± 0.05, 0.88 ± 0.06 and 1.09 ±± 0.05 MPa, from left to right, with the transducer driven at 85 mVpp. All foci appeared at the same location in the y-axis as in the simulation and presented a maximum difference in pressure of 40% (Fig. 2-(b)).

The temperature-time profile for the iso-thermal lens is shown Fig 2-(d). Maximum focal peak temperatures were 48.0 ± 0.1, 48.7 ± 0.1 and 47.2 ± 0.1 °C, from left to right, corresponding to mean TIDs values of 56 ± 5, 54 ± 4 and 54 ± 3 CEM$_{43}$ respectively. Comparison of the mean TID in the central well with the others, gives a relative difference of 3.7% for the one located to its left, and 0.03% to its right.

To study spheroids response to ultrasound-delivered hyperthermia, the iso-thermal lens was used as its thermal field was more suitable for this purpose. Five spheroids were exposed

Authorized licensed use limited to: UNIVERSIDAD POLITECNICA DE VALENCIA. Downloaded on February 24,2025 at 15:23:24 UTC from IEEE Xplore. Restrictions apply.

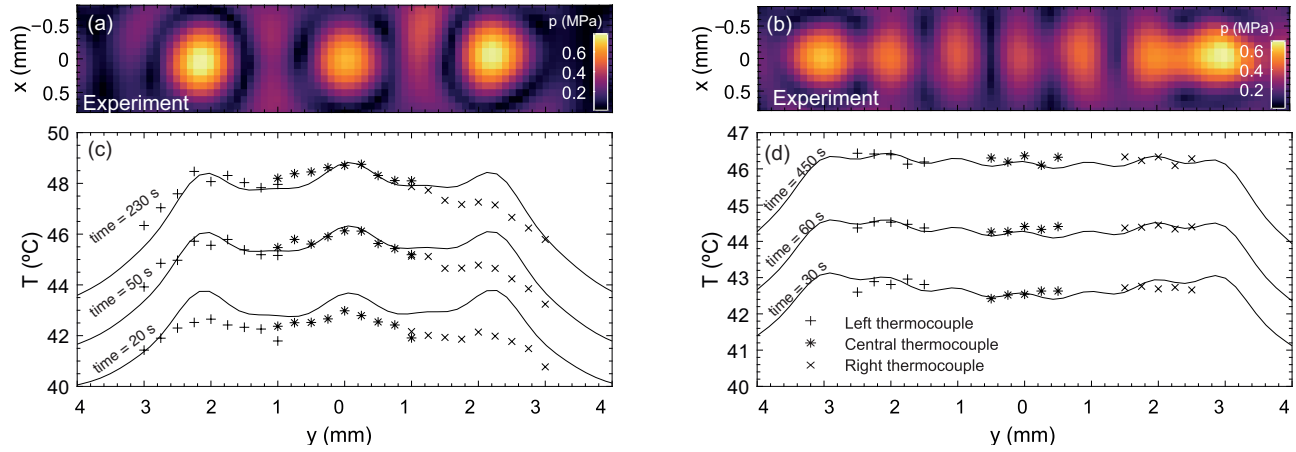



Fig. 2. (Experimental acoustic pressure field in the x-y plane at z = 40 mm for (a) the iso-pressure and (b) the iso-thermal hologram. Temperature profile at different time points simulated (solid line) and measured experimentally with each thermocouple for (c) the iso-pressure and (d) the iso-thermal hologram.

and retrieved for each TID of 7.5, 30 and 60 $CEM_{43}$, while three were successfully exposed to 120 $CEM_{43}$ and eight were sham-exposed. Fig 3-(a) and (b) show the evolution of a sham-exposed spheroid and other treated with 120 $CEM_{43}$ thermal dose. Sham- and 7.5 $CEM_{43}$ ultrasound-exposed spheroids continued to grow, increasing their size by approximately 40 $\pm$ 4% by the end of the study (10 days). Spheroids exposed to a TID of 120 $CEM_{43}$ presented a contraction 15 $\pm$ 6%, while no difference in size was seen at 30 or 60 $CEM_{43}$. Thermocycler-heated spheroids presented no shrinkage even at the highest thermal dose.

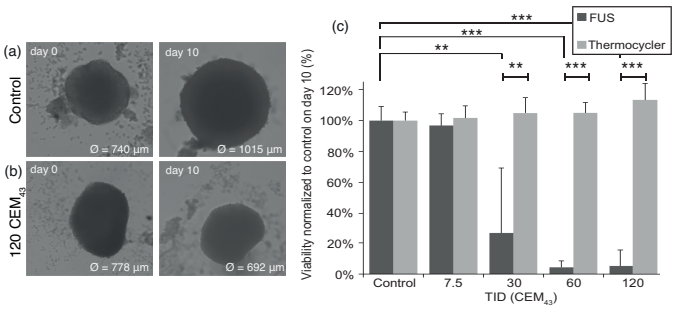



Fig. 3. ((a) Images of a control spheroid and (b) a 120 $CEM_{43}$ treated spheroid on days 0 (day of treatment) and 10.(c) Viability study on day 10 after treatment for ultrasound and thermocycler- heated spheroids. Results are presented as mean $\pm$ SD and statistical significance is denoted with asterisk: (*) $p \leq 0.05$, (**), $p \leq 0.01$, (***), $p \leq 0.001$.

U87-MG spheroids exposed to ultrasound showed greater reduction in growth than those treated with a thermocycler. Considering the same TID in both cases, thermocycler-heated spheroids did not present a significant size reduction compared to sham-exposed, having statistically significant difference in size for all TIDs compared with ultrasound-heated spheroids. Their viability was also studied on the day 10 after treatment. A statistically significant reduction in spheroid metabolic activity when exposed to ultrasound with TIDs of 30, 60 and 120 $CEM_{43}$ (with relative viability of 27 $\pm$ 42%, 4 $\pm$ 2% and 5 $\pm$ 10%, respectively compared to sham-exposed spheroids), while we didn't see any statistically significant difference in TIDs of 7.5 $CEM_{43}$ (97 ± 4%) compared to sham exposed spheroids. Thermocycler-heated spheroids showed no significant viability changes when exposed to any of the studied TIDs. Significant differences (p ¡ 0.05) are seen when comparing the viability of ultrasound-exposed spheroids with thermocycler-heating for TIDs of 30, 60 and 120 $CEM_{43}$ (Fig. 3-(c)).

## IV. Discussion and Conclusions

Differences on the TID achieved with the iso-pressure strategy were of $\pm$ 37 $CEM_{43}$ over the three thermocouples, located at each of the spheroids location. With the iso-thermal strategy, this difference was lowered to $\pm$ 1.3 $CEM_{43}$, achieving a uniform TID over the three wells. This was reached by tuning the lens not to an acoustic field but to a predefined thermal dose. The spheroid holder designed in this work allowed to expose three tumour aggregations at the same time with real-time temperature and TID control. Exposing spheroids with this system to TIDs of 30 to 120 $CEM_{43}$ resulted in reduced spheroid growth, associated with lower metabolic activity (viability), compared to both sham exposed controls and thermocycler-heated spheroids.

The system presents several limitations that need to be assessed. One of the was the difficulty when retrieving the spheroids from the holder due to the similar colour of the spheroids and the phantom, resulting in a loss of 25 % of them. Also, each time the spheroids were pipetted in and out the wells, the phantom was degraded and needed to be changed. Another limitation is that the spheroids were exposed to a non sterile environment during the experiment, even though they were manipulated and placed in the holder in an sterile manner.

Nevertheless, this system based on a holographic lens designed to deliver a uniform TID allow to simultaneously expose complex targets or over relatively wide regions to a

Authorized licensed use limited to: UNIVERSIDAD POLITECNICA DE VALENCIA. Downloaded on February 24,2025 at 15:23:24 UTC from IEEE Xplore. Restrictions apply.

uniform TID. Also, in combination with the spheroid holder system, can contribute to a reduction in the use of research animals in in-vivo experiments as it provides an inexpensive, reliable, and quick method of exposing tumour spheroids to ultrasound heating. Also, the system can be very useful in the research of combined ultrasound heating and radiotherapy. Further work could be carried out to optimize thermal uniformity in different complex 2D or even 3D targets, by, for example, applying optimization and machine learning algorithms [23] to accurately engineer the acoustic wavefront and produce uniform thermal patterns for ultrasound hyperthermia systems.

## REFERENCES


[1] H. P. Kok, E. N. Cressman, W. Ceelen, C. L. Brace, R. Ivkov, H. Grüll, G. Ter Haar, P. Wust, and J. Crezee, "Heating technology for malignant tumors: A review," *International Journal of Hyperthermia*, vol. 37, no. 1, pp. 711–741, 2020.

[2] G. ter Haar and C. Coussios, "High intensity focused ultrasound: physical principles and devices," *International journal of hyperthermia*, vol. 23, no. 2, pp. 89–104, 2007.

[3] M. Tillander, S. Hokland, J. Koskela, H. Dam, N. P. Andersen, M. Pedersen, K. Tanderup, M. Ylihautala, and M. Köhler, "High intensity focused ultrasound induced in vivo large volume hyperthermia under 3d mri temperature control," *Medical physics*, vol. 43, no. 3, pp. 1539–1549, 2016.

[4] A. Partanen, M. Tillander, P. S. Yarmolenko, B. J. Wood, M. R. Dreher, and M. O. Köhler, "Reduction of peak acoustic pressure and shaping of heated region by use of multifoci sonications in mr-guided high-intensity focused ultrasound mediated mild hyperthermia," *Medical physics*, vol. 40, no. 1, p. 013301, 2013.

[5] W. Chu, R. M. Staruch, S. Pichardo, M. Tillander, M. O. Köhler, Y. Huang, M. Ylihautala, M. McGuffin, G. Czarnota, and K. Hynynen, "Magnetic resonance–guided high-intensity focused ultrasound hyperthermia for recurrent rectal cancer: Mr thermometry evaluation and preclinical validation," *International Journal of Radiation Oncology* Biology* Physics*, vol. 95, no. 4, pp. 1259–1267, 2016.

[6] E. Ozhinsky, V. A. Salgaonkar, C. J. Diederich, and V. Rieke, "Mr thermometry-guided ultrasound hyperthermia of user-defined regions using the exablate prostate ablation array," *Journal of therapeutic ultrasound*, vol. 6, no. 1, pp. 1–10, 2018.

[7] G. Maimbourg, A. Houdouin, T. Deffieux, M. Tanter, and J.-F. Aubry, "3d-printed adaptive acoustic lens as a disruptive technology for transcranial ultrasound therapy using single-element transducers," *Physics in Medicine & Biology*, vol. 63, no. 2, p. 025026, 2018.

[8] S. Jiménez-Gambín, N. Jiménez, J. M. Benlloch, and F. Camarena, "Holograms to focus arbitrary ultrasonic fields through the skull," *Physical Review Applied*, vol. 12, no. 1, p. 014016, 2019.

[9] Z. Ma, A. W. Holle, K. Melde, T. Qiu, K. Poeppel, V. M. Kadiri, and P. Fischer, "Acoustic holographic cell patterning in a biocompatible hydrogel," *Advanced Materials*, vol. 32, no. 4, p. 1904181, 2020.

[10] J. Kim, S. Kasoji, P. G. Durham, and P. A. Dayton, "Acoustic holograms for directing arbitrary cavitation patterns," *Applied Physics Letters*, vol. 118, no. 5, p. 051902, 2021.

[11] S. Jiménez-Gambín, N. Jiménez, A. N. Pouliopoulos, J. M. Benlloch, E. E. Konofagou, and F. Camarena, "Acoustic holograms for bilateral blood-brain barrier opening in a mouse model," *IEEE Transactions on Biomedical Engineering*, vol. 69, no. 4, pp. 1359–1368, 2021.

[12] D. Andrés, J. Vappou, N. Jiménez, and F. Camarena, "Thermal holographic patterns for ultrasound hyperthermia," *Applied Physics Letters*, vol. 120, no. 8, p. 084102, 2022.

[13] B. M. Baker and C. S. Chen, "Deconstructing the third dimension–how 3d culture microenvironments alter cellular cues," *Journal of cell science*, vol. 125, no. 13, pp. 3015–3024, 2012.

[14] P. X. Mouratidis, I. Rivens, J. Civale, R. Symonds-Tayler, and G. Ter Haar, "Relationship between thermal dose and cell death for ?rapid? ablative and ?slow? hyperthermic heating," *International Journal of Hyperthermia*, vol. 36, no. 1, pp. 228–242, 2019.

[15] P. X. Mouratidis, I. Rivens, and G. Ter Haar, "A study of thermal dose-induced autophagy, apoptosis and necroptosis in colon cancer cells," *International Journal of Hyperthermia*, vol. 31, no. 5, pp. 476–488, 2015.

[16] S. C. Brüningk, I. Rivens, C. Box, U. Oelfke, and G. Ter Haar, "3d tumour spheroids for the prediction of the effects of radiation and hyperthermia treatments," *Scientific Reports*, vol. 10, no. 1, p. 1653, 2020.

[17] . C. Coussios, C. Farny, G. Ter Haar, and R. Roy, "Role of acoustic cavitation in the delivery and monitoring of cancer treatment by high-intensity focused ultrasound (hifu)," *International journal of hyperthermia*, vol. 23, no. 2, pp. 105–120, 2007.

[18] P. Mishra, M. Hill, and P. Glynne-Jones, "Deformation of red blood cells using acoustic radiation forces," *Biomicrofluidics*, vol. 8, no. 3, p. 034109, 2014.

[19] D. Andrés, I. Rivens, P. Mouratidis, N. Jiménez, F. Camarena, and G. Ter Haar, "Holographic focused ultrasound hyperthermia system for uniform simultaneous thermal exposure of multiple tumor spheroids," *Cancers*, vol. 15, no. 9, p. 2540, 2023.

[20] B. E. Treeby and B. T. Cox, "k-wave: Matlab toolbox for the simulation and reconstruction of photoacoustic wave fields," *Journal of biomedical optics*, vol. 15, no. 2, pp. 021314–021314, 2010.

[21] S. A. Sapareto and W. C. Dewey, "Thermal dose determination in cancer therapy," *International Journal of Radiation Oncology* Biology* Physics*, vol. 10, no. 6, pp. 787–800, 1984.

[22] H. H. Pennes, "Analysis of tissue and arterial blood temperatures in the resting human forearm," *Journal of Applied Physiology*, vol. 1, no. 2, pp. 93–122, 1948.

[23] T. Fushimi, K. Yamamoto, and Y. Ochiai, "Acoustic hologram optimisation using automatic differentiation," *Scientific reports*, vol. 11, no. 1, pp. 1–10, 2021.


Authorized licensed use limited to: UNIVERSIDAD POLITECNICA DE VALENCIA. Downloaded on February 24,2025 at 15:23:24 UTC from IEEE Xplore. Restrictions apply.